# Improved confinement induced by tangential injection of compact torus into the Saskatchewan Torus-Modified (STOR-M) tokamak

C. Xiao, A. Hirose, and S. Sen

Citation: Physics of Plasmas **11**, 4041 (2004); doi: 10.1063/1.1768177
View online: http://dx.doi.org/10.1063/1.1768177
View Table of Contents: http://scitation.aip.org/content/aip/journal/pop/11/8?ver=pdfcov
Published by the AIP Publishing



# Improved confinement induced by tangential injection of compact torus into the Saskatchewan Torus-Modified (STOR-M) tokamak

C. Xiao and A. Hirose
*Plasma Physics Laboratory, Department of Physics & Engineering Physics, University of Saskatchewan, Saskatoon, Saskatchewan S7N 5E2, Canada*

S. Sen[a)]
*Research School of Physical Science and Engineering, The Australian National University, Canberra, ACT 0200, Australia*

(Received 23 February 2004; accepted 10 May 2004; published online 19 July 2004)

Compact torus injection into the Saskatchewan Torus-Modified [Phys. Fluids B **4**, 3277 (1992)] tokamak discharges has triggered improved confinement characterized by an increase in the electron density by more than twofold, 30% reduction in the $H_\alpha$ radiation level, significant suppression of floating potential fluctuations and $m=2$ Mirnov oscillations. In this paper, we present detailed experimental setup and results, as well as an extended theory explaining the mechanism for triggering improved confinement in a tokamak by compact torus injection. © *2004 American Institute of Physics.* [DOI: 10.1063/1.1768177]

## I. INTRODUCTION

Central fuelling of a tokamak reactor can significantly improve tokamak confinement as demonstrated in pellet-enhanced performance.[1] Localized central fuelling provides a means to control the plasma density and pressure profiles which may also enhance bootstrap current density leading to modification of magnetic shear in the plasma core. In a tokamak reactor, central fuelling is desired to achieve a high fuel burn-up rate and low tritium recycling. The conventional fuelling technologies used in the present-day tokamaks include peripheral gas admission and frozen pellet injection. Typical launch speed of the pellets is less than 10 km/s. For high field side injection, the launch speed is also restricted by the need for the pellets to be guided through tubes.[2] The relatively low pellet speed prevents the pellets from direct fuel deposition beyond the separatrix in a reactor-grade tokamak such as International Thermonuclear Experimental Reactor (ITER).[3] Energetic neutral beam injection used for plasma heating and current drive is economically inefficient for the fuelling purpose. Developing alternative fuelling technologies is urgently needed for the next generation tokamaks to achieve central fuelling.

Compact torus (CT) injection as an emerging technology to centrally fuel a tokamak reactor was originally proposed by Perkins *et al.*[4] and Parks.[5] CT is a doughnut-shaped high density plasmoid confined by the self-organized intrinsic magnetic field with both toroidal and poloidal components, a magnetic field configuration similar to that in a tokamak. Such structurally robust CTs can be formed and accelerated with coaxial electrodes in an injector similar to those used in the ring accelerator experiment (RACE) (Ref. 6) and the compact toroid fueller (CTF) for the Tokamak de Varennes (TdeV).[7,8] CTs have been routinely accelerated to hundreds of kilometers per second. Early CT injection experiments carried out on the Caltech's ENCORE tokamak[9] resulted in a current increase due to helicity injection, a large increase in the electron density, and a major disruption due to excessive fuelling. The first nondisruptive CT injection experiment was achieved in TdeV with CTF.[7] The experiments on TdeV showed negligible impurity injection and some signatures of improved confinement of the tokamak plasma.[8] The penetration depth inferred from the multichannel interferometer density measurements on TdeV qualitatively confirmed that the required CT kinetic energy density was approximately proportional to the tokamak magnetic field energy density as predicted by Perkins *et al.*[4,5] In both ENCORE and TdeV experiments, CTs were injected at the normal injection angle from the low field side. Some theoretical studies show that tangential CT injection has longer interaction time with the tokamak plasma and might cause smaller disturbance on the tokamak discharge.[10,11] In addition, tangential CT injection may transfer CT momentum to tokamak plasma to induce and sustain toroidal rotation, which has beneficial effects on stabilizing the locked mode and resistive wall mode.[12] At the University of Saskatchewan, it has been observed that tangential CT injection into the Saskatchewan Torus-Modified (STOR-M) tokamak induces *H*-mode discharges. In JAERI Fusion Torus-2M (JFT-2M),[13] a medium size tokamak, nondisruptive injection has been achieved with an injector built at the Himeji Institute of Technology.[14] CTs have also been injected into the *H*-mode discharges in JFT-2M. The CT injection experiments on the Texas Experimental Tokamak-Upgrade (TEXT-U) (Ref. 15) using the Caltech's CT injector have revealed that the configuration of the acceleration electrodes in the drift tube in the vicinity of the tokamak toroidal field greatly affects the CT penetration performance. The experiments have also shown that this adverse effect can be minimized by modifications of the acceleration electrodes and the drift tube.[16] Along with experimental studies, a con-

[a)]Also at Hampton University, Virginia, USA and Delhi University, Delhi, India.

 

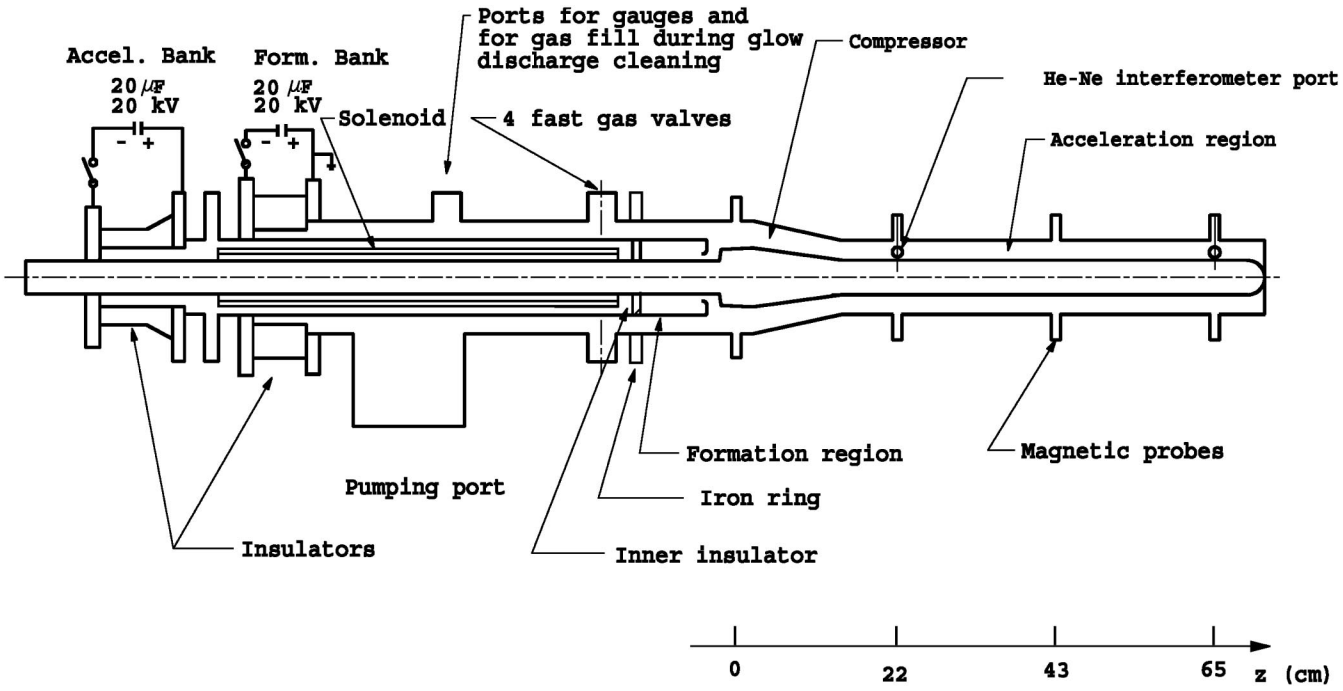


FIG. 1. Schematic diagram of USCTI.

ceptual design of an injector capable of fuelling the ITER tokamak was also proposed.[17]

In an earlier paper,[18] we presented the main experimental results of the improved confinement induced by tangential CT injection into STOR-M and a theoretical explanation of the triggering mechanism based on the shear and curvature of the toroidal plasma flow. This paper will provide more details on the the experimental setup and results, and an extended version of the theoretical studies related to the mechanism for *H*-mode triggering without a shear in the radial electric field. In Sec. II the detailed experimental setup, including the University of Saskatchewan Compact Torus Injector (USCTI) and the STOR-M parameters, will be described. In Sec. III, the features of the *H*-mode-like discharges induced by CT injection into STOR-M will be presented. The extension of theoretical studies on the mechanism of the *H*-mode triggered by toroidal flow shear will be discussed in Sec. IV. A brief summary will be provided in Sec. V.

## II. EXPERIMENTAL SETUP

### A. USCTI injector

Figure 1 shows the sketch of the USCTI. USCTI has a coaxial configuration with formation, compression, and acceleration sections. Compact toroids are formed and accelerated in the following sequences. Initially, a capacitor bank discharge through a solenoid induced a quasisteady state bias magnetic field in the region between the inner and outer formation electrodes. The rise time of the solenoid bank discharge is $\approx 1$ ms. Due to the edge effects the magnetic field lines penetrate both inner and outer formation electrodes, providing footprints for the formation discharge. Four electromagnetic fast-acting gas valves located symmetrically about the injector axis inject hydrogen gas into the formation region. The gas puffing valves were located at either $z=-29$ cm in the preliminary injection experiments or $z=-18$ cm in the improved experiments. It has been found that moving the gas valves closer to the formation region ($z=-18$ cm) can reduce 80% the gas puffing amount and still ensure a reliable gas breakdown under our experimental conditions. To ensure a symmetric CT formation, the amount of gas puffing through each of four valves has been carefully equalized. An adequate time delay has been allowed for the gas to diffuse evenly into the formation region before the formation discharge is initiated to ionize the gas and to supply a current through the plasma. The return current through the inner formation electrode produces a toroidal (azimuthal) magnetic field in the plasma. When the formation discharge current is high enough, the force induced by the cross product between the radial current and the toroidal magnetic field, $\mathbf{J}\times\mathbf{B}$, pushes the plasma forward and stretches the bias magnetic field lines provided by the solenoid. When the field lines are stretched to such an extent that the magnetic field lines reconnect behind the plasma, a free CT is formed. The reconnected bias magnetic field originated from the solenoid magnetic field forms the CT's poloidal field. The CT eventually relaxes to a minimum energy state.[19] Finally, the acceleration discharge accelerates the CT along the acceleration electrodes to a high speed.

Two identical capacitor banks (20 $\mu$F, up to 30 kV) are used for consecutive formation and acceleration discharges. A compressor region reduces the diameter of the outer electrode from 15 cm in the formation region to 10 cm in the acceleration region. The diameter of the inner acceleration electrode is 3.6 cm.

To minimize impurities in CTs, all electrode surfaces in contact with the CT plasma are coated with refractory mate-

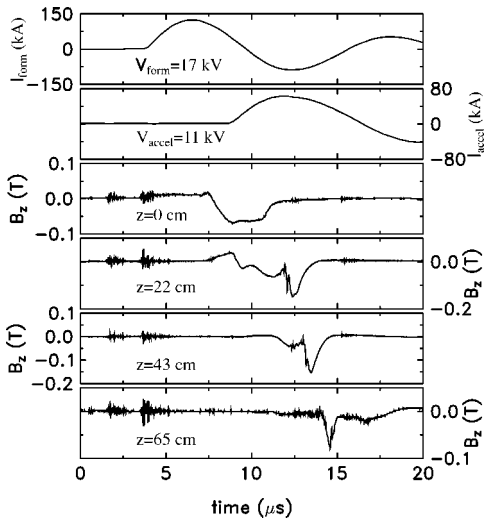


FIG. 2. Typical USCTI discharge current wave forms and CT poloidal (axial) magnetic fields measured at four axial locations.

rials, either tungsten or chromium. To further reduce CT impurities caused by outgassing from the chamber wall, on-line baking maintains the electrode temperature about 100 °C. In addition, alternating current (60 Hz) glow discharge cleaning is also employed as needed.

Magnetic probe arrays are used to measure both poloidal and toroidal magnetic fields in the USCTI injector at four axial locations ($z=0$, 22, 43.5, 65 cm as shown in Fig. 1). A He-Ne laser interferometer of Michelson configuration is employed to measure the plasma density at two axial locations ($z=22$, 65 cm), where two sets of magnetic probes on the accelerator are also located. The CT velocity and length can be inferred from the time delay and pulse width of the magnetic field signals measured at three axial locations in the accelerator section. The typical CT parameters near the exit of the injector are: 15 cm in length, $(1-4)\times10^{15}$ cm$^{-3}$ in density, and $\approx150$ km/s in velocity. The CT mass is $\approx1$ $\mu$g, corresponding to 50% the particle inventory in the STOR-M discharges.

Figure 2 shows the wave forms of the CT formation and acceleration discharge currents and the CT magnetic field signals measured at four axial locations. In this particular shot, the formation and acceleration capacitor banks were charged to 17 kV and 11 kV, respectively. The gas puffing valves were located at $z=-18$ cm. Since USCTI is small in size for injection experiments on the STOR-M tokamak, fast discharge circuits with low inductance have been designed to ensure that the CT can be accelerated to the desired velocity within the first half cycle of current along a relatively short acceleration section. In the formation region at $z=0$ cm, the magnetic field signal is relatively wide. At the entrance of the acceleration region at $z=22$ cm, this broad signal feature remains for about several microseconds. When the acceleration current approaches the peak value at $t=12$ $\mu$s, a sudden increase in the magnetic field occurs and a short pulse emerges, indicating that a free CT is entering the acceleration region at a high speed. At the locations $z=43.5$ cm and $z=65$ cm, the magnetic field signal pulse remains short, indicating that the CT does not expand in length while it is moving forward along the acceleration electrodes.

### B. Set up of injection experiments

The STOR-M tokamak is a small research tokamak with an iron core transformer. The minor and major radii are 12 cm and 46 cm, respectively. The shape of the stainless steel limiter used in STOR-M combines two parallel plates and two circular sections. The two horizontal bars are located 12 cm from the tokamak center. The circular sections with a radius of 13 cm are located in the inboard and outboard of the tokamak. This arrangement allows the plasma column to move $\pm1$ cm in the horizontal direction without being scrapped off. STOR-M is also equipped with a horizontal position feedback control system. The plasma is heated ohmically only. Hydrogen gas was used for both CT and tokamak discharges in all experiments reported in this paper.

The injector was connected to the STOR-M tokamak via bellows so that the injection angle could be varied. The experiments reported in this paper were carried out at an injection angle of 27° with respect to the local major radius direction as shown in Fig. 3. The tokamak plasma parameters were monitored with various diagnostic tools during the CT injection experiments. A 4 mm microwave interferometer, offset from the CT injection port by $\phi=22.5°$ in the toroidal direction, was used to measure the electron density averaged along the central vertical chord. A spectrometer aiming horizontally through the center of the discharge was employed to monitor the $H_\alpha$ emission intensity at $\phi=-112.5°$ (not shown in the diagram). This arrangement reduced the variation of the emission intensity caused by plasma horizontal displacement which often occurred during the $H$-mode-like discharges induced by CT injection into STOR-M. A rake probe array was installed through a horizontal port at $\phi=22.5°$ to measure either the electron density or the floating potentials at the plasma edge. A set of Mirnov coils outside the chamber wall at $\phi=-67.5°$ was used to monitor $m=2$ and $m=3$ MHD activities. The nominal plasma parameters were: $B_t=0.7-0.8$ T, $I_p=20-25$ kA, and $n_e=(0.5-2)\times10^{13}$ cm$^{-3}$.

## III. EXPERIMENTAL RESULTS

### A. Preliminary injection experiments

During the preliminary CT injection experiments on STOR-M, the gas valves on USCTI were located at $z=-29$ cm. The CT velocities were about 100 km/s. The magnetic field in the STOR-M tokamak was 0.7 T. Figure 4 shows the STOR-M tokamak discharge parameters with a CT injected at $t=16.5$ m after the start of the tokamak discharge. The traces in Fig. 4 are, from top to bottom, the tokamak discharge current, loop voltage, line-averaged electron density, plasma horizontal displacement, and the $H_\alpha$ radiation level. After CT injection, there is no change in the STOR-M discharge current. The loop voltage remains almost unchanged in the initial 3 ms after CT injection before it shows a transient drop followed by an increase. Since plasma current remains constant, the loop voltage drop may be at-

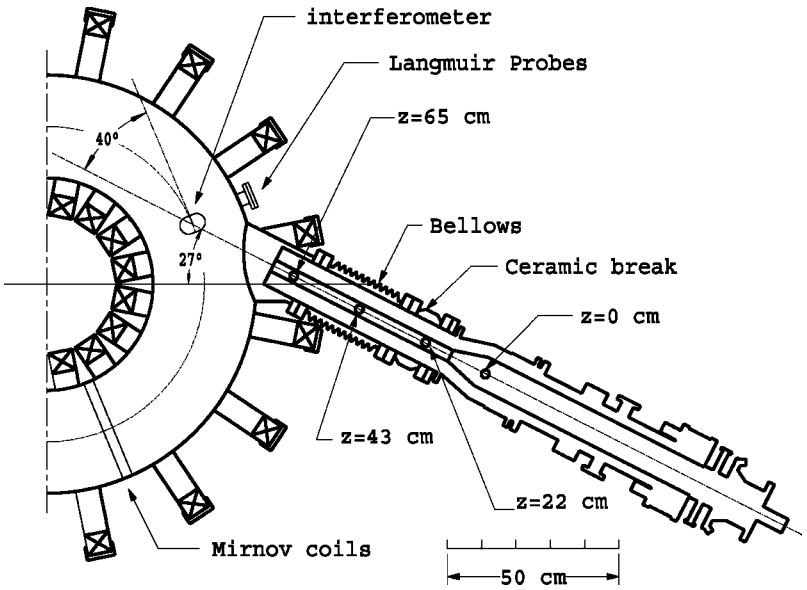


FIG. 3. Arrangement of CT injection experiments on the STOR-M tokamak.

tributed to either a heating or current drive effect. However, no conclusion has been drawn from the preliminary CT injection experiments since the loop voltage drop were brief and this did not occur in later experiments. The most significant change is the rapid electron density increase starting about 1 ms after CT injection. The density doubles from $9\times10^{18}$ m$^{-3}$ to $1.8\times10^{19}$ m$^{-3}$ within 3 ms, representing a density increase rate of $3\times10^{21}$ m$^{-3}$/s. It is also interesting to notice that the plasma position starts to move outwards at the time when the density starts to increase. The experimental observations seem to suggest an increase in the thermal energy content in the STOR-M tokamak discharge which caused the outward displacement. It should be pointed out that the current in the vertical field coil increased in an attempt to restore the plasma horizontal position. However, the response time of the feedback control circuit was not fast enough to do so. The last trace in Fig. 4 shows that the $H_\alpha$ drops immediately following the CT injection and lasted about 2 ms. The drop did not seem to be significant because the decrease was only 1 bit in our digitizer.

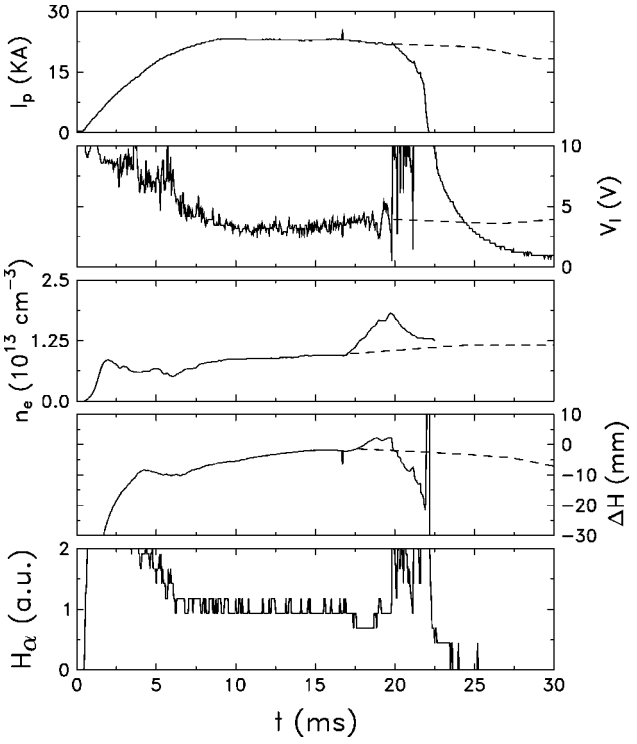


FIG. 4. Wave forms of plasma parameters in a STOR-M tokamak discharge during the preliminary CT injection experiments.

It is clear that the CT injection has induced many interesting phenomena in the STOR-M discharge. However, a major disruption always follow several milliseconds after the CT injection. In the following subsection, we will show the results of the disruption-free $H$-mode-like discharges induced by CT injection into STOR-M.

### B. *H*-mode-like tokamak discharges induced by CT injection

Following the preliminary CT injection experiments on STOR-M, the gas puffing valves on the USCTI injector was moved from $z=-29$ cm to $z=-18$ cm. Since the gas is puffed closer to the formation discharge region, a much smaller amount of gas puffing provides the adequate instantaneous gas pressure for reliable formation discharge breakdown. The reduction of the gas puffing was as high as 80%, reducing significantly the amount of trailing gas entering the STOR-M tokamak. In addition, the toroidal magnetic field in STOR-M was increased from 0.7 T in the preliminary CT injection experiments to 0.8 T in the later experiments described in the rest of the paper. The higher toroidal magnetic field made the STOR-M discharge more stable against disruptions. The smaller amount of trailing gas following the CT plasmoid prevented excess neutral gas fuelling. As a result, disruption-free CT injection was achieved. Furthermore, phenomena of $H$-mode-like confinement induced by CT injection into STOR-M became more evident, allowing more detailed studies.

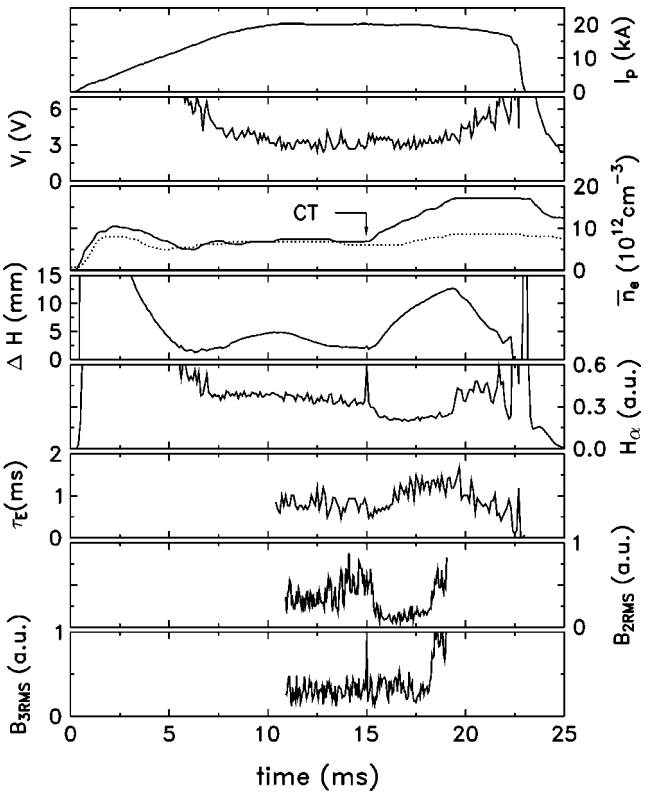


FIG. 5. Wave forms of plasma parameters in a STOR-M tokamak discharge during the disruption-free CT injection experiments.

Figure 5 shows the waveform of the parameters of a tokamak discharge with a CT injected at $t=15$ ms. The traces shown are (from top): plasma current, loop voltage, line averaged electron density, horizontal displacement, $H_\alpha$ radiation intensity, the global energy confinement time, and the rms levels of the $m=2$ and $m=3$ MHD oscillations. Following the CT injection, the discharge current and loop voltage remain almost intact, indicating a constant Spitzer temperature. The electron density increases more than twofold from $0.75\times10^{13}$ to $1.7\times10^{13}$ cm$^{-3}$ at a rate of $\approx1.9\times10^{21}$ cm$^{-3}$/s. Slower density increase rate, compared with those in the preliminary CT injection experiments, may be attributed to reduced trailing gas fuelling. The high density phase remains until the end of the discharge. For comparison, the electron density for a tokamak discharge without initiating the CT discharge but with gas puffing into the CT injector is also superimposed on the density trace (dotted line). In this case, the density starts to increase about 2 ms after the time when the CT would be injected. The density increase is also much smaller compared with the case with CT injection. The next trace shows the plasma horizontal displacement. Accompanying the increase in the total thermal energy content in the plasma column, the plasma position shifts outwards during the time between $t=15$ ms and $t=20$ ms. The $H_\alpha$ radiation level decreases abruptly by $\approx30\%$ following the CT injection and returns to the nominal level at $t=20$ ms, indicating an L-H transition and an H-L back transition, respectively. The $m=2$ MHD oscillation level decreases after the CT injection and starts to recover at $t=18$ ms to its original level before CT injection. In contrast to the $m=2$ oscillations, the $m=3$ MHD oscillation level remains intact before $t=18$ ms. Both $m=2$ and $m=3$ oscillation levels start to increase at $t=18$ ms, which might be the precursor for H-L back transition at $t=20$ ms. The dominant frequency component of the magnetic fluctuations is $\approx25$ kHz.

The global energy confinement time has been estimated from the temperature $T_\sigma$ based on anomalous Spitzer conductivity and the line averaged density $n_e$ using the following formula:

$$\tau_E=\frac{2n_eT_\sigma}{I_pV_l+P_{CT}},$$

where $I_pV_l$ is the ohmic heating power and $P_{CT}$ the power input due to CT injection. The ion temperature in STOR-M has been assumed to be $T_\sigma/3$. We also assumed that the CT energy was deposited at the rate of

$$P_{CT}=\frac{E_{CT}}{\tau_1-\tau_2}[\exp(-t/\tau_1)-\exp(-t/\tau_2)],$$

where $E_{CT}=58$ J is the sum of the estimated kinetic (11 J) and magnetic (47 J) energies in CT. $\tau_2=0.5$ ms and $\tau_1=3$ ms characterize the times for the deposited power to reach the peak and to diminish, respectively. For this particular set of parameters, the power reaches a peak value of 13 kW at $t=1$ ms after CT injection and diminishes to about 20% the peak value at $t=5$ ms. As shown in Fig. 5, the global energy confinement time increases from 0.9 ms (prior to CT injection) to 1.4 ms maximum. Since the electron temperature does not change significantly, the increase in the global energy confinement time has been attributed to the improved particle confinement.

Figure 6 shows the rms levels of the potential fluctuations, measured with the rake probes, at $r=11,11.4,12.2,13.6$ cm across the scrape-off layer (SOL) and the edge region. The running rms averages were performed over ten data points or 50 $\mu$s. In both SOL and the edge region, the floating potential fluctuation levels decrease significantly after CT injection. The reduction in the floating potential fluctuation levels coincides with the following phenomena: (a) reduction in $H_\alpha$ radiation intensity, (b) increase in electron density, and (c) plasma outward displacement.

The electron density and floating potential profiles at the STOR-M edge region were measured using the rake probe array. Figure 7 shows the time history of the electron density at the plasma edge and SOL. The solid lines indicate the case with CT injection (shot number 21 194) at $t=16$ ms. The dotted lines are for the case without CT discharge (but with gas puffing into the injector). For comparison, the history of the line-averaged density for the corresponding discharges has been also depicted in the lower panel in Fig. 7. Compared with the case without CT injection, CT injection causes larger and more prompt increases in both local and line-average densities. Figure 8 depicts, for the case with CT injection, the density profiles at various times for the discharge (shot number 21 194) shown in Fig. 7. The density decreases initially after the CT injection and then increases. The density profile becomes more steepened in the rest of the

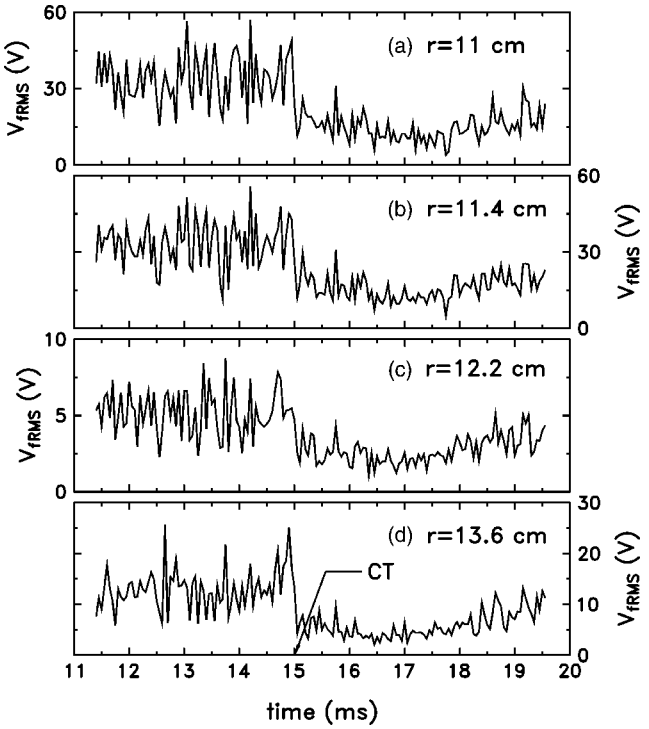


FIG. 6. Suppression of floating potential fluctuations during an improved discharge induced by CT injection at $t=15$ ms.

improved confinement phase. After $t=21$ ms, the edge density profiles gradually return to that before CT injection although the line-averaged electron density remains high without further increase.

Figure 9 shows the time history of the floating potentials at $r=10.9$, 11.3, 12, and 13.5 cm and Fig. 10 the profiles of the floating potential at times $t=15$, 17, 19, and 21 ms for the same discharge. In this discharge, the CT was injected at $t=15$ ms. It can be seen that the CT injection causes a prompt increase in the potential at all measured locations. The duration of the potential increase generally agrees with

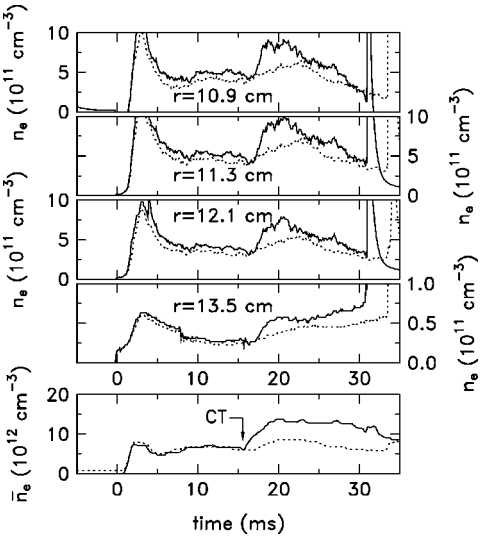


FIG. 7. Time history of the electron density in the tokamak edge and SOL regions.

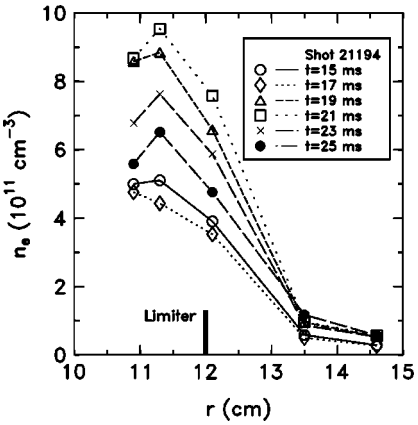


FIG. 8. Profiles of the electron density in the tokamak edge and SOL regions.

the duration during which the $H$-mode-like discharge phenomena occur (increase in density, suppression of floating potential fluctuations, and $m=2$ Mirnov oscillations). Since the floating potential change is not significant, the radial electric field does not undergo noticeable change as shown in Fig. 10.

## IV. THEORETICAL MODEL

In our earlier work we proposed that the transport barrier may be created by purely parallel flow profile.[18] We demonstrated that the parallel flow curvature stabilizes dissipative drift-ballooning modes and this might be the mechanism responsible for the $H$-mode transition in the STOR-M. However, we have not considered any temperature gradient driven instability. Here, we extend our earlier work to the toroidal ITG modes, which is thought to be the likely mechanism for anomalous transport in the plasma.

We use usual $(r,\theta,\phi)$ coordinates, corresponding to the minor radial, poloidal, and toroidal directions, respectively, and consider the long-wavelength ($\kappa^2 a_i^2 \ll 1$) ITG modes for a large aspect-ratio circular tokamak. The perturbed potential can then be expressed as

$$\tilde{\varphi}(r,\theta,\phi,t)=\varphi(r,\theta)\exp\{i(n\phi-m\theta-\omega t)\},$$

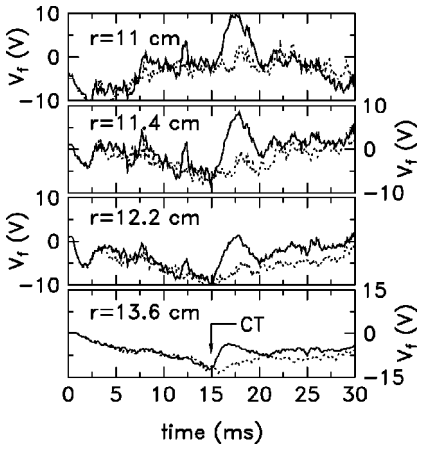


FIG. 9. Time history of the floating potential in the tokamak edge and SOL regions.

where $r$ is the radial distance from the mode rational surface, i.e., $m=nq(r_0)$, and $s=rq'/q$ at $r=r_0$. Here, for simplicity, we will assume ions to be cold and will ignore the electron temperature gradient. Using fluid descriptions, the eigenvalue equation in the presence of a velocity field can be derived in a straightforward way:

$$a_i^2\frac{\partial^2\tilde{\varphi}}{\partial r^2}-b\tilde{\varphi}+\frac{(\omega_*-\omega+i\omega\delta)}{\left[\omega+\omega_*\left(\frac{1+\eta_i}{\tau}\right)\right]}\tilde{\varphi}-\left(\frac{\omega_*\epsilon_c}{\omega\kappa a_i}\right)^2\left(\frac{\partial}{\partial\theta}+i\kappa sr\right)^2\tilde{\varphi}-2\epsilon_n\frac{\omega_*}{\omega}\left(\cos\theta+\frac{i\sin\theta}{\kappa}\frac{\partial}{\partial r}\right)\tilde{\varphi}+\frac{\kappa a_i c_s k_\parallel}{\left[\omega+\omega_*\left(\frac{1+\eta_i}{\tau}\right)\right]\omega}\frac{\partial V_{\parallel 0}(r)}{\partial r}\tilde{\varphi}=0, \tag{1}$$

where

$$\kappa=nq/r=m/r,$$
$$s=(r/q)(dq/dr),$$
$$a_i^2=c^2m_iT_e/e^2B^2,$$
$$c_s^2=T_e/m_i,$$
$$b=\kappa^2a_i^2,$$
$$\epsilon_n=q\epsilon_c=r_n/R,$$
$$\tau=T_e/T_i,$$
$$\omega_*=(\kappa cT_e/eBr_n),$$
$$\nabla_\parallel\tilde{\varphi}=ik_\parallel\tilde{\varphi},$$
$$\nabla_\parallel=\frac{1}{qR}\left(\frac{\partial}{\partial\theta}+q\frac{\partial}{\partial\phi}\right).$$

Now to model the equilibrium parallel velocity we follow the toroidal velocity profile usually observed during the VH-mode, the NCS-mode, and the RI-mode experiments:

$$v_{\parallel o}(r)=v_{\parallel 00}-\left(\frac{r}{L_{v1}}+\frac{r^2}{L_{v2}^2}\right)v_{\parallel 0},$$

where

$$\frac{dv_{\parallel 0}}{dr}=-\frac{v_{\parallel 00}}{L_{v1}},\quad \frac{1}{2}\frac{d^2v_{\parallel 0}}{dr^2}=-\frac{v_{\parallel 00}}{L_{v2}^2}.$$

We put

$$x=\kappa rs\Rightarrow r=\frac{x}{\kappa s}\Rightarrow\frac{\partial r}{\partial x}=\frac{1}{\kappa s},$$
$$\frac{\partial}{\partial x}=\frac{\partial}{\partial r}\frac{\partial r}{\partial x}\Rightarrow\frac{1}{\kappa s}\frac{\partial}{\partial r}\Rightarrow\frac{\partial}{\partial r}=\kappa s\frac{\partial}{\partial x},$$
$$\frac{\partial^2}{\partial x^2}=\frac{1}{(\kappa s)^2}\frac{\partial^2}{\partial r^2},$$
$$\frac{\partial^2}{\partial r^2}=(\kappa s)^2\frac{\partial^2}{\partial x^2}.$$

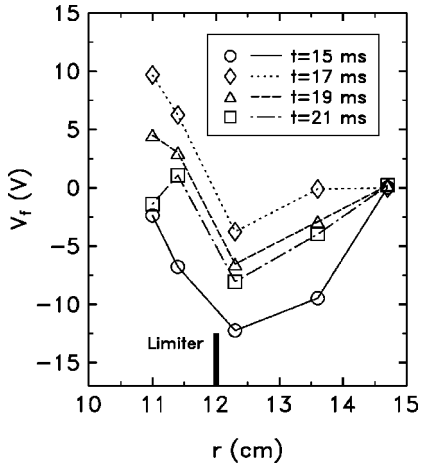


FIG. 10. Profiles of the floating potential in the tokamak edge and SOL regions.

Therefore we get

$$\left[\frac{\partial^2}{\partial x^2}-\sigma^2\left(\frac{\partial}{\partial\theta}+ix\right)^2-\epsilon\left(\cos\theta+is\sin\theta\frac{\partial}{\partial x}\right)+\lambda+\frac{\kappa a_i c_s x}{bs^2qR\omega\left[\omega+\omega^*\left(\frac{1+\eta_i}{\tau}\right)\right]}\times\left(-\frac{v_{\parallel 00}}{L_{v1}}-\frac{v_{\parallel 00x}}{\kappa sL_{v2}^2}\right)\right]\tilde{\varphi}=0, \tag{2}$$

where $\sigma=\epsilon_c/(bs)$, $\epsilon=(2\epsilon_n)/bs^2$, and $v_{\parallel 0}$ is the equilibrium parallel flow. The first term in Eq. (1) arises from the finite Larmor radius effect and the third from the ion sound. The parameter $i\delta$ represents the destabilizing effect of electron Landau resonance and the trapped electrons. The fourth is the effect of toroidal coupling. Parallel flow has two effects. First, it introduces a Doppler shift $k_\parallel v_{\parallel 0}$ [in deriving Eq. (1) we have neglected Doppler shifts due to equilibrium velocity] in all time derivatives, and second, an extra term $v_E\nabla v_{\parallel 0}(x)$ representing the radial convection of the ion momentum. It is the second term which makes the effect of parallel flow shear completely different from that of perpendicular flow shear.

To reduce the two-dimensional (2D) eigenmode problem to 1D, we will apply the ballooning transformation. However, the validity of the conventional ballooning formalism in the presence of sheared flow is, in general, severely restricted. This is due to the fact that in an equilibrium with differential rotation, the Doppler-shifted frequencies varies from one flux surface to another and hence the conventional ballooning formalism, for which to the lowest order (the local approximation) the perturbation is a superposition of *identical* single helicity modes, no longer applies. In other

words, the eikonal solutions do not have pure exponential time dependence and are not eigenmodes in the system. However, we notice that the spatial variation in the Doppler shift $k_{\|}v_{\|0}$ in the mode frequency due to *parallel* flow is negligible for flute-type modes ($k_{\|} \ll k_{\perp}$). It is probably obvious as $d^n/dx^n[k_{\|}v_{\|0}(x)] \ll d^n/dx^n[k_{\perp}v_0(x)]$ due to the fact that $k_{\|} \ll k_{\perp}$ and that $v_{\|0} \sim v_{\perp 0}$ in the experiments. So, one can eliminate the Doppler shift by performing a Galilean transformation in the $\hat{e}_{\|}$ direction. This has been noted elsewhere. It can be noted that the effect of the parallel shear/curvature enters in the problem through an extra term $v_E \nabla v_{\|0}(x)$ representing radial convection of ion momentum. So, once radial variation in the Doppler shift is neglected, the restriction on the applicability of the ballooning formalism no longer applies.

To determine the radial mode structure, the solution of the fully 2D eigenmode problem must be obtained within the framework of ballooning formalism, this means solving the problem to a higher order. The problem then separates into two distinctive radial length scales. To leading order, the problem reduces to the usual 1D eigenmode equation (with radial variable appearing only as parameter), which determines the mode structure along the magnetic field lines. The next order equation then determines the radial mode structure. In the usual theory of high $n$ ballooning mode, one maps the poloidal angle $\theta$ on to an extended coordinate $\chi$ with $-\infty < \chi < \infty$ and writes the perturbation in the form

$$\tilde{\varphi}(\theta,x) = \sum_m e^{-im\theta} \int_{-\infty}^{\infty} e^{im\chi} \hat{\phi}(\chi,x) d\chi,$$

where $\hat{\phi} = A(x)F(\chi,x)\exp[-ix(\chi+\chi_0)]$. Here $\chi_0$ is an arbitrary phase of the eikonal. $A(x)$ is assumed to vary on some scale intermediate between the equilibrium scale length and the perpendicular wavelength. Now to leading order (in $n^{-1/2}$ expansion), the ballooning equation becomes

$$\left( \sigma^2 \frac{d^2}{d\chi^2} + (\chi+\chi_0)^2 + \epsilon[\cos\chi + s(\chi+\chi_0)\sin\chi] + p_1 x + p_2 x^2 - \lambda \right) F(\chi,x) = 0. \tag{3}$$

To explore its implication for radial mode structure and stability of toroidal ITG mode one needs the higher order ballooning theory. In the higher order theory $\chi_0$ is obtained from the equation $(\partial\lambda/\partial\chi_0)(x,\chi_0) = 0$ and $A(x)$ satisfies

$$\frac{\partial^2\lambda}{\partial\chi_0^2} \frac{d^2A}{dx^2} + [2(\lambda-\lambda_0) - 2p_1 x - 2p_2 x^2]A = 0, \tag{4}$$

where

$$\lambda = \frac{1}{bs^2}\left[ \frac{\omega_* - \omega - i\omega\delta}{\omega - \omega_*\left(\frac{1+\eta_i}{\tau}\right)} - b \right],$$

$$\lambda_0 = i\frac{\epsilon_c}{bs},$$

$$p_1 = \frac{\kappa a_i c_s v_{\|00}}{bs^2 L_{v1} qR\omega\left[\omega + \omega_*\left(\frac{1+\eta_i}{\tau}\right)\right]},$$

$$p_2 = \frac{a_i c_s v_{\|00}}{bs^3 L_{v2}^2 qR\omega\left[\omega + \omega_*\left(\frac{1+\eta_i}{\tau}\right)\right]}.$$

Equation (2) is a simple Weber equation. When $p_2$ is positive and $\partial^2\lambda/\partial\chi_0^2 > 0$ ($\partial^2\lambda/\partial\chi_0^2 > 0$ is necessary in order that the mode be most unstable), $A(x)$ is localized Gaussian function. However, an important change is introduced by the velocity term for the negative magnetic shear. $A(x)$ is then given by

$$A(x) = \exp\left[ -i\frac{1}{2}\left( |p_2| \Big/ \left|\frac{\partial^2\lambda}{\partial\chi_0^2}\right| \right)^{1/2} (x+x_0)^2 \right], \tag{5}$$

where $x_0 = p_1/|p_2|$. So, the mode envelop is now radially outgoing, which is reminiscent of the equivalent slab problem. Velocity curvature in the toroidal problem like magnetic shear in the corresponding slab problem creates an *antiwell* in the radial direction. The wave energy is therefore convected outward. The eigenvalue is given by

$$\lambda = \lambda_0 + \frac{p_1^2}{2|p_2|} - i\frac{1}{2}\left( |p_2| \left|\frac{\partial^2\lambda}{\partial\chi_0^2}\right| \right)^{1/2}. \tag{6}$$

This also shows damping contribution in the global eigenvalue. Thus, both the radially outgoing nature and the damping contribution in the global eigenvalue unambiguously show that parallel flow profile might act to stabilize toroidal ITG waves which otherwise escape magnetic shear damping!

## V. DISCUSSIONS

In light of apparent absence of the radial electric field induced poloidal flow shear during the improved confinement induced by CT injection, we have explored the role of the parallel flow profile in the improved confinement. We have therefore shown in this article that the transport barriers may be created by purely parallel flow profile. We have demonstrated that the curvature in the parallel flow stabilizes toroidal ITG modes, which have been identified as the likely mechanism for anomalous transport in the plasma. We thus demonstrate two aspects. First, in regards to the confinement improvement, the important role of the toroidal rotation may not be only through the $\mathbf{E}\times\mathbf{B}$ shear (which is usually weak and this is exactly what is seen on STOR-M), but also through the strong parallel component. Second, as the parallel flow in the tokamak is almost equal to the toroidal flow and as the toroidal flow can be generated by the NBI, there is no limit for how long the parallel flow can be maintained.

So, the transport barrier created by the toroidal flow will have a distinctive advantage over that created by the poloidal flow as the toroidal flow unlike the poloidal counterpart is not damped by the magnetic pumping.

## VI. SUMMARY

In summary, the *H*-mode-like discharges triggered by CT injection in the STOR-M tokamak are accompanied by an increase in the electron density, significant reduction in the $H_\alpha$ radiation level, steepening of the edge density profile, suppression of the $m=2$ Mirnov oscillations, and suppression of the floating potential fluctuations. These features are similar to those associated with the *H* modes induced with edge turbulent heating or by electrode/limiter biasing observed earlier in STOR-M.[20] In contrast to the edge turbulent heating induced *H* mode in STOR-M, the floating potential at the plasma edge and SOL increases during the improved confinement phase. Another interesting point of observation is the lack of appreciable change in the equilibrium radial electric field during the transition to the improved mode. A theory is proposed to show that it is indeed possible to form a transport barrier by purely parallel flow curvature which means no change in the perpendicular flow (hence, in the radial electric field) is necessary.

## ACKNOWLEDGMENTS

Technical assistance provided by D. McColl, P. Balon, B. Chomyshen, and G. Ehlert is acknowledged with gratitude. Fruitful discussions with Dr. R. Raman are appreciated.

This work was sponsored by the Canada Research Chair Program and Natural Sciences and Engineering Research Council of Canada.

[1] P. Smeulders, L. C. Appel, B. Balet *et al.*, Nucl. Fusion **35**, 225 (1995).
[2] P. T. Lang, B. Alper, L. R. Baylor *et al.*, Nucl. Fusion **42**, 388 (2002).
[3] ITER Physics Basis Editors, ITER Physics Expert Group Chairs and Co-Chairs, and ITER Joint Central Team and Physics Integration Unit, Nucl. Fusion **39**, 2137 (1999).
[4] L. J. Perkins, J. H. Ho, and J. H. Hammer, Nucl. Fusion **28**, 1365 (1988).
[5] P. B. Parks, Phys. Rev. Lett. **61**, 1364 (1988).
[6] J. H. Hammer, C. W. Hartman, and J. L. Eddleman, Phys. Rev. Lett. **61**, 2843 (1988).
[7] R. Raman, F. Martin, B. Quirion *et al.*, Phys. Rev. Lett. **73**, 3101 (1994).
[8] R. Raman, F. Martin, E. Haddad *et al.*, Nucl. Fusion **37**, 967 (1997).
[9] M. R. Brown and P. M. Bellan, Phys. Rev. Lett. **64**, 2144 (1990).
[10] S. V. Bozhokin, Sov. J. Plasma Phys. **16**, 702 (1990).
[11] C. Xiao, A. Hirose, and W. Zawalski, Nucl. Fusion **38**, 249 (1998).
[12] A. Bondson and D. J. Ward, Phys. Rev. Lett. **72**, 2709 (1994).
[13] The JFT-2M Group, Y. Miura, F. Okano, N. Suzuki, M. Mori, K. Hoshino, T. Takizuka, K. Itoh, and S.-I. Itoh, Phys. Plasmas **3**, 3696 (1996).
[14] T. Ogawa, N. Fukumoto, M. Nagata *et al.*, Nucl. Fusion **39**, 1911 (1999).
[15] G. Cima, R. V. Bravenec, A. J. Wootton, T. D. Rempel, F. Gandy, C. Watts, and M. Kwon, Phys. Plasmas **2**, 720 (1995).
[16] J. Yee and P. M. Bellan, Nucl. Fusion **38**, 711 (1998).
[17] P. Giersewski, R. Raman, and D. Hwang, Fusion Technol. **28**, 619 (1995).
[18] S. Sen, C. Xiao, A. Hirose, and R. A. Cairns, Phys. Rev. Lett. **88**, 185001 (2002).
[19] J. B. Taylor, Phys. Rev. Lett. **33**, 1139 (1974).
[20] W. Zhang, C. Xiao, and A. Hirose, Phys. Fluids B **5**, 3961 (1993).